ELSEVIER

Contents lists available at ScienceDirect

### Journal of Hydrology

journal homepage: www.elsevier.com/locate/jhydrol



#### Technical Note



# Modeling vapor transfer in soil water and heat simulations: A modularized, partially-coupled approach

Zhuangji Wang <sup>a,b</sup>, Dennis Timlin <sup>a,\*</sup>, David Fleisher <sup>a</sup>, Wenguang Sun <sup>a,c</sup>, Sahila Beegum <sup>a,c</sup>, Sanai Li <sup>a</sup>, Yan Chen <sup>d</sup>, Vangimalla R. Reddy <sup>a</sup>, Katherine Tully <sup>b</sup>, Robert Horton <sup>e</sup>

- <sup>a</sup> Adaptive Cropping System Laboratory, USDA-ARS, Beltsville, MD 20705, USA
- b Department of Plant Science and Landscape Architecture, University of Maryland, College Park, MD 20742, USA
- <sup>c</sup> Nebraska Water Center, University of Nebraska, Lincoln, NE 68588, USA
- <sup>d</sup> Department of Soil and Water Science, China Agricultural University, Beijing 100193, China
- e Department of Agronomy, Iowa State University, Ames, IA 50011, USA

#### ARTICLE INFO

This manuscript was handled by Jiri Simunek, Editor-in-Chief, with the assistance of Giuseppe Brunetti, Associate Editor

Keywords: Vapor transfer Water and heat transfer Modularization Numerical simulations 2DSOII.

#### ABSTRACT

Coupled water and heat transfer models are widely used to analyze soil water content and temperature dynamics, evaluate agricultural management systems, and support crop growth modelling. In relatively dry soils, vapor transfer, rather than liquid water flux, becomes the main pathway for water redistribution. However, in some modularized soil simulators, e.g., 2DSOIL (Timlin et al., 1996), vapor transfer is not included, which may induce errors in soil water and heat modelling. Directly embedding vapor transfer into existing water and heat transfer modules may violate the modularized architecture of those simulators. Therefore, the objectives of this study are to design a vapor transfer model, evaluate its performance, and implement it as a separate module in a coupled soil water and heat simulator, e.g., 2DSOIL. The efficacy of the vapor transfer model is evaluated by comparing the simulated soil water content and temperature before and after including the new vapor transfer model, and the soil water content and temperature simulated with the standard Philip and de Vries (1957) model. By implementing vapor transfer as a separate module in 2DSOIL, modifications to existing water and heat transfer modules can be minimized and the modularized model architecture can be maintained. Numerical examples of 2DSOIL with the new vapor transfer model are presented to illustrate the effects of vapor flux on soil water and temperature redistributions. In conclusion, the new vapor transfer model provides an effective and easy-to-use method to account for the effects of vapor transfer on coupled soil water and heat simulations.

#### 1. Introduction

Numerical simulation is an important approach to elucidate water and heat transfer in soil, and it supports a wide range of applications in agriculture and civil engineering. For model establishment, a variety of soil simulators, e.g., the early versions of HYDRUS such as HYDRUS-1D or CHAIN-2D (Simunek and van Genuchten, 1994; Simunek et al., 2012), combined the Richards equation (Richards, 1931) and a conduction–convection heat equation as the governing model to represent the water and heat transfer in soil [see Eq. (1)]. Such a model formulation does not include temperature gradient as a factor in liquid water flux [see Eq. (1a)]. After solving the Richards equation [i.e., Eq. (1a)], the liquid water flux can be considered as a known quantity when computing the conductive and convective heat transfer [see Eq. (1b)],

where liquid water flux carries sensible heat flux. Thus, given a discretized time step, the two equations for soil water transfer and soil heat transfer [Eq. (1a) and (1b), respectively] can be solved one-by-one using relatively simple and efficient numerical implementations. Based on that model formulation [Eq. (1)], soil water and heat transfer can be programed into two separate modules, which can also support a relatively complex but flexible model architecture. For example, in 2DSOIL (Timlin et al., 1996), a modularized simulator of soil physical and chemical processes in 2D soil profiles (one horizontal scale and one vertical scale), both the water transfer module and the heat transfer module can establish their own connections (i.e., dataflow pathways) to soil surface water and heat balance models, crop growth models, and soil-root interaction models. Additional modules can be linked to the water and heat transfer modules in 2DSOIL with minimal or no

E-mail address: dennis.timlin@usda.gov (D. Timlin).

 $<sup>^{\</sup>ast}$  Corresponding author.

modifications to the existing modules (Timlin et al., 1996; Kim et al., 2012; Wang et al., 2021a; Wang et al., 2021b). However, vapor transfer, which contributes to both water and heat dynamics in soil, is not included, and that may induce errors in the simulations of soil water content and temperature.

In relatively dry soils, vapor transfer is the predominant means for water redistribution, which also contributes to sensible and latent heat fluxes (Scanlon, 1994; Scanlon and Milly, 1994; Zeng et al., 2009a; Zeng et al., 2009b). The reasons are (I) in relatively dry soils, relatively large temperature gradients can serve as a driving force for vapor transfer, and (II) a relatively large fraction of soil pores are air-filled, providing pathways for vapor transfer. However, adding vapor transfer to existing soil water and temperature models may substantially increase the model complexity, because (I) vapor transfer has effects on both water fluxes and heat fluxes, and (II) phase changes of soil water must be considered. For example, Philip and de Vries (1957) and de Vries (1958) included the vapor transfer, as well as the associated heat fluxes and water phase changes, and then, the water transfer model and the heat transfer model became fully coupled [see Eq. (2)].

The Philip and de Vries (1957) model is widely used in simulating coupled water and heat transfer in porous media, and multiple improvements have been proposed. For example, Sophocleous (1979) and Milly (1982) reformulated the Philip and de Vries (1957) model using matric potential to account for the hysteresis and the coupling of matric potential and temperature, and Nassar and Horton (1989, 1997) included osmotic potential and developed a coupled heat, water, and solute transfer model for wettable soils. However, under the coupled formulation [Eq. (2)], the water transfer and heat transfer models cannot be solved one-by-one within a given discretized time step, which causes difficulties in modularization. Solving the two equations in the Philip and de Vries (1957) model [Eq. (2)] one-by-one can greatly enhance the computing efficiency and simplify the programming. Thus, multiple studies have investigated alternative formulations that can achieve such a "one-by-one" approach. For example, Saito et al. (2006) and Šimůnek et al. (2016) illustrated a commonly used simplification that for each discretized time step, first assume soil temperature is constant and solve for soil water content, second assume soil water content is constant and solve for soil temperature, and repeat those two steps in the following discretized time steps. Such a simplification method has been adopted in a variety of related studies, such as the coupled water and heat transfer in partially frozen soil (Zheng et al., 2021) and the water-heat-air models with surface evaporation (Zeng et al., 2011a; Zeng et al., 2011b), although the governing models in those studies were not exactly the same as the original version of the Philip and de Vries (1957) model [Eq. (2)] but were adapted to their specific application scenarios. However, for modularized soil simulators with connections to climate, soil surface, and crop models, such as 2DSOIL, adding the vapor transfer to the water and heat transfer model with such a simplification is still challenging. That is because the inclusion of vapor transfer can induce relatively large modifications to both existing water and heat transfer modules, as well as the dataflow pathways between water and heat modules and other existing modules. Therefore, there exists a need to design an approach to implement vapor transfer that can be compatible with modularized soil simulators, such as 2DSOIL, where vapor transfer is not originally considered.

The objectives of this study are (I) to design a model for vapor

transfer, as well as the associated sensible and latent heat fluxes and water phase changes, and make it compatible with modularized soil simulators, (II) to evaluate the performance of the new vapor transfer model, and (III) to implement the vapor transfer model as a separate module in coupled soil water and heat simulators, such as 2DSOIL. Following these objectives, vapor transfer simulations can be enabled in 2DSOIL and modifications to the 2DSOIL model architecture, the dataflow pathways, and the existing water and heat transfer modules should be minimized. Moreover, additional flexibility can be provided by such modularization, which allows independent controls on the water transfer in liquid and vapor phases. For example, the vapor transfer pathway can be artificially activated or deactivated based on user settings. If two soil layers are separated by a semi-permeable film, e.g., Tyvek (DuPont Inc., water-repellent but permeable to gas flux), the semi-permeable film can be simply implemented as an impermeable boundary for liquid water flux in the water transfer module, while in the vapor transfer module, such a semi-permeable boundary exerts no effect.

#### 2. Model establishment

#### 2.1. Review of existing models

The combination of the Richards equation (Richards, 1931) and the conduction–convection heat equation is shown in Eq. (1). Within a given discretized time step, water and heat transfer can be solved one-by-one using the two equations in Eq. (1). Because vapor transfer and associated sensible and latent heat fluxes are not included, it may produce undesirable simulation results in relatively dry soils. In the following sections, Eq. (1) (without vapor transfer in soil) is referred to as the "preliminary formulation  $(M_{\rm prel})$ ", and it serves as the starting point for our vapor transfer model design, which means we will develop a vapor transfer model and insert the vapor transfer model in  $M_{\rm prel}$  using a modularized manner.

$$\begin{cases} \text{Water Equation}: & \frac{\partial \theta}{\partial t} = \nabla \cdot \left[ \underbrace{K(h,T)\nabla h}_{=-q_l(h,T)} \right] \\ \text{Heat Equation}: & C_s \frac{\partial T}{\partial t} = \nabla \cdot [\lambda \nabla T] - \nabla \cdot [c_l \rho_l q_l (T-T_0)] \end{cases}$$
 (1a)

Equation (1a) presents the mass conservation of soil liquid water, where  $\theta(\text{cm}^3\ \text{cm}^{-3})$  is the volumetric water content; h(cm) is the soil matric potential;  $K(h,T)(\text{cm s}^{-1})$  is the unsaturated hydraulic conductivity. A constitutive relation between  $\theta$  and h can be provided using the water characteristic function. Equation (1b) presents the conservation of energy, where T(K) is the soil temperature;  $C_s(J\ \text{cm}^{-3}\ \text{K}^{-1})$  is the soil volumetric heat capacity;  $\lambda(W\ \text{cm}^{-1}\ \text{K}^{-1})$  is the thermal conductivity;  $c_l \approx 4.187\ \text{J g}^{-1}\ \text{K}^{-1}$  and  $\rho_l \approx 1.0\ \text{g cm}^{-3}$  are the specific heat and density of liquid water;  $q_l = -K(h)\nabla h(\text{cm s}^{-1})$  is the Darcy flux density;  $T_0(K)$  is a pre-specified reference temperature. Hence,  $c_l\rho_lq_l(T-T_0)$  represents the sensible heat flux associated with liquid water flux.

In contrast to the preliminary formulation  $(M_{\text{prel}})$ , the Philip and de Vries (1957) model, which fully couples the water and heat transfer in soil and includes water transfer in both liquid and vapor phases, is shown in Eq. (2).

Water Equation: 
$$C_{\theta\theta} \frac{\partial h}{\partial t} + C_{\theta T} \frac{\partial T}{\partial t} = \nabla \cdot \left[ \underbrace{D_{mv}(h,T)\nabla h + D_{tv}(h,T)\nabla T}_{=-q_t(h,T)} + \underbrace{K(h,T)\nabla h + D_{tl}(h,T)\nabla T}_{\equiv -q_t(h,T)} \right]$$

$$= \nabla \cdot \left[ \left[ D_{mv}(h,T) + K(h,T) \right] \nabla h + \left[ D_{tv}(h,T) + D_{tl}(h,T) \right] \nabla T \right] \qquad (2a)$$
Heat Equation: 
$$C_{T\theta} \frac{\partial h}{\partial t} + C_{TT} \frac{\partial T}{\partial t} = -\nabla \cdot \left[ -\lambda \nabla T + c_l \rho_l q_l (T - T_0) + \left[ L_0 \rho_l q_v + c_v \rho_l q_v (T - T_0) \right] \right]$$

$$= c_{th}(h,T) \qquad (2b)$$

 $C_{\theta\theta}(\mathrm{cm}^{-1}),\ C_{\theta T}(\mathrm{K}^{-1}),\ C_{T\theta}(\mathrm{J\ cm}^{-3}\ \mathrm{cm}^{-1})$  and  $C_{TT}(\mathrm{J\ cm}^{-3}\ \mathrm{K}^{-1})$  are capacity coefficients for h and T with respect to the changes in soil water content and temperature. In Eq. (2a),  $D_{mv}(h,T)(\mathrm{cm\ s}^{-1})$  and  $D_{tv}(h,T)(\mathrm{cm}^2\ \mathrm{s}^{-1}\ \mathrm{K}^{-1})$  are coefficients of vapor transfer under the water potential gradient and temperature gradient, respectively; therefore,  $q_v(\mathrm{cm\ s}^{-1})$  is the total vapor flux driven by both gradients. Similarly,  $D_{tl}(h,T)(\mathrm{cm}^2\ \mathrm{s}^{-1}\ \mathrm{K}^{-1})$  in Eq. (2a) is the liquid water diffusion coefficient under temperature gradient; combined with the Darcy flow defined in Eq. (1a),  $q_l(h,T)$  represents the total liquid water flux. In Eq. (2b),  $L_0(\mathrm{J}\ \mathrm{g}^{-1})$  is the heat of vaporization of water at  $T_0$ ;  $c_v\approx 1.864(\mathrm{J}\ \mathrm{g}^{-1}\ \mathrm{K}^{-1})$  is the specific heat of vapor. Hence,  $L_0\rho_lq_v+c_v\rho_lq_v(T-T_0)$  represents the latent and sensible heat fluxes carried by vapor, relative to the internal energy of liquid water at  $T_0$ , and  $q_h(h,T)$  becomes the total heat flux in soil.

The numerical implementation of the Philip and de Vries (1957) model, without the simplifications illustrated in Saito et al. (2006), has been evaluated with experimental and numerical studies, under a variety of initial and boundary conditions, e.g., Nassar and Horton (1997), Heitman et al. (2007), Heitman et al. (2008) and Wang et al. (2017). Thus, such a numerical approach of the Philip and de Vries (1957) model

quires solving a relatively large linear system that contains both h and T values from the computing girds. Saito et al. (2006) and Šimůnek et al. (2016) illustrated a simplification that can solve the two equations in Eq. (2) one-by-one. That is, within a given discretized time step, first assume T is constant and update h, and second assume h is constant and update T. Therefore, h and T are updated in two steps. A diagram for such a twostep process is presented in Zheng et al. (2021) [See Fig. 1 for the dataflow chart in Zheng et al. (2021). We note that there exist some variations in the Hydrus-based models. E.g., one improvement is that Zheng et al. (2021) repeat the "one-by-one" procedure in solving h and T twice within one time step, but h and T are still updated in the "water flow" and "heat flow" blocks separately]. However, because of the simplification, the corresponding governing model was slightly changed from Eq. (2) to enable the "one-by-one" approach. The equation system is presented as Eq. (2'). In the following sections, we denote the Philip and de Vries (1957) model, with the numerical approach illustrated in Saito et al. (2006) and Šimůnek et al. (2016), as the "simplified formulation  $(M_{\text{simp}})$  ". Because the governing models that use Saito et al. (2006) and Šimůnek et al. (2016) simplification vary based on specific application scenarios, the formulation of Eq. (2') may not be exactly the same as the ones in Saito et al. (2006), Šimůnek et al. (2016), Zeng et al. (2011a), Zeng et al. (2011b) or Zheng et al. (2021).

$$\begin{cases} \textit{Water Equation}: C_{\theta\theta} \frac{\partial h}{\partial t} = \nabla \cdot [[D_{mv}(h,T) + K(h,T)] \nabla h + [D_{tv}(h,T) + D_{tl}(h,T)] \nabla T], \frac{\partial T}{\partial t} = 0 \text{(2a')} \\ \textit{Heat Equation}: C_{TT} \frac{\partial T}{\partial t} = -\nabla \cdot [-\lambda \nabla T + c_l \rho_l q_l (T - T_0) + [L_0 \rho_l q_v + c_v \rho_l q_v (T - T_0)]], \frac{\partial h}{\partial t} = 0 \text{(2b')} \end{cases}$$

[Eq. (2)] is used as a "standard reference point" in this study, and in the following sections, it is referred to as the "full formulation  $(M_{\rm full})$ ".  $M_{\rm full}$  also serves as the target in this study, which means that after implementing a vapor transfer model in  $M_{\rm prel}$  [recall  $M_{\rm prel}$  is the starting point of our model design where vapor transfer is not originally included, see Eq. (1)], the soil water and temperature simulations should achieve a performance similar to  $M_{\rm full}$ .

The standard derivations of the Philip and de Vries (1957) model and the computation of capacity, hydraulic conductivity and diffusivity coefficients can be found in Heitman et al. (2008) and Wang et al. (2017). The soil thermal conductivity ( $\lambda$ ) is adopted from Lu et al. (2014) and summarized in Table 1; the expression of the liquid water diffusion coefficient [ $D_{tt}(h,T)$ ] is simplified from Groenevelt and Kay (1974) and Milly (1982), which is provided in Appendix A. We also note that although both liquid water and water vapor are considered, the Philip and de Vries (1957) model is not a typical 2-phase model but a 1.5-phase model because water potential and thermal equilibrium is assumed at the water–vapor interface (Vanderborght et al., 2017).

Typically, within a given time step, the full formulation  $M_{\text{full}}$  assumes that h and T are updated together as one equation system, which re-

#### 2.2. The vapor transfer model

In this study, the vapor transfer model is designed as a rebalance of soil water and heat by vapor flux, and it should be solved after  $M_{\rm prel}$  to include the vapor transfer and its effects on heat exchanges [recall that  $M_{\rm prel}$  is treated as the starting point of our model design]. The vapor transfer model can be simply described in the following two steps. First, taking the difference between the right-hand side of Eqs. (1) and (2) and assuming  $D_{tl}(h,T)\ll D_{tv}(h,T)$ , i.e., the thermally driven liquid water transfer is much smaller than the vapor flux in an agricultural field soil (see Appendix A for detailed adjustment), the vapor fluxes and the sensible and latent heat flux associated with vapor transfer can be extracted. Second, reassemble the extracted vapor fluxes and vapor-induced heat fluxes to the left-hand side of Eq. (2), where the left-hand side of Eq. (2) represents the differentiation of total soil water and total soil heat with respect to time. Then, we obtain the governing equation for the vapor transfer model, as shown in Eq. (3).

**Table 1**Physical Properties of the Soil in Section 2.3.

Ida (fine-silty, mixed, superactive, calcareous, mesic Typic Udorthents)			
Soil Textural Properties			
Sand $(f_{sand}, g g^{-1})$	0.022		
Silt $(f_{silt}, g g^{-1})$	0.729		
Clay $\left(f_{clay}, \mathrm{g} \; \mathrm{g}^{-1}\right)$	0.249		
Organic matter (g g <sup>-1</sup> )	0.044		
Specific surface area $(S_a, cm^2 cm^{-3})$	$2.44\times10^6$		
Bulk density $(\rho_b, g \text{ cm}^{-3})$	1.20		
Hydraulic Properties			
Saturated water content $(\theta_s, \text{cm}^3 \text{ cm}^{-3})$	0.547		
Saturated hydraulic conductivity at $T_0(K_s, \text{cm s}^{-1})$	$3.80 \times 10^{-5}$		
Water characteristic function	$h = -13.0 \times (\theta/\theta_s)^{-6.53}$		
Hydraulic conductivity $(K, cm s^{-1})$	$K = \left[\mu(T_0)/\mu(T)\right] \times (\theta/\theta_s)^{16.06} K_s \dagger$		
Thermal Properties			
Thermal conductivity $(\lambda,$	$\lambda = 0.01 ig( \lambda_{dry} + \exp(eta -  heta^{-lpha}) ig)$		
$W \text{ cm}^{-1} \text{ K}^{-1}$ ) (Lu et al., 2014)	$\lambda_{dry} = -0.56 heta_s + 0.51$		
	$\alpha = 0.67 f_{clay} + 0.24$		
$\dagger \mu(T)$ represents the dynamic viscosity	$\beta=1.97f_{sand}+1.87\rho_b-1.36f_{sand}\rho_b-0.95$ y of water, as a function of soil temperature.		

**Table 2** Initial and Boundary Conditions in Illustrative Example 1.

			· · · · · · · · · · · · · · · · · · ·
(a)	Initial Condition		$ heta=0.15, T=25^{\circ} ext{C}$
	<b>Boundary Condition</b>	Left	$q_l=0, q_ u=0, T=25^\circ ext{C}$
		Right	$q_{l} = 0, q_{ u} = 0, T = 30^{\circ} \mathrm{C}$
(b)	Initial Condition		$ heta=0.15, T=25^{\circ} ext{C}$
	<b>Boundary Condition</b>	Left	$q_l = 0, q_{\nu} = 0, q_h = -0.0001 \mathrm{W \ cm^{-2}}$
		Right	$q_l=0, q_\nu=0, q_h=0.0001 W~{\rm cm}^{-2}$
(c)	Initial Condition		$ heta=0.2, T=25^{\circ} ext{C}$
	<b>Boundary Condition</b>	Left	$ heta=0.2, T=25^{\circ} ext{C}$
		Right	$q_l = 0, q_{\nu} = -1 \times 10^{-7} \text{cm s}^{-1}, T = 30^{\circ} \text{C}$
(d)	Initial Condition		$ heta=0.15, T=25^{\circ} ext{C}$
	<b>Boundary Condition</b>	Left	$ heta=0.20, T=25^{\circ} ext{C}$
		Right	$ heta=0.10, T=30^{\circ} ext{C}$

$$\begin{cases} \text{Vapor Equation}: C_{\theta\theta} \frac{\partial h}{\partial t} + C_{\theta T} \frac{\partial T}{\partial t} = \nabla \cdot [D_{mv}(h, T) \nabla h + D_{tv}(h, T) \nabla T] & \text{(3a)} \\ \text{Heat Equation}: C_{T\theta} \frac{\partial h}{\partial t} + C_{TT} \frac{\partial T}{\partial t} = -\nabla \cdot [L_0 \rho_l q_v + c_v \rho_l q_v (T - T_0)] & \text{(3b)} \end{cases}$$

Equation (3) can be implemented as a separate module, which needs to be solved after  $M_{\rm prel}$ . The initial conditions of Eq. (3) are the same as the initial conditions of  $M_{\rm prel}$ , and zero water flux and zero heat flux are assumed as the boundary conditions, as shown in Eq. (4).

$$\begin{cases} D_{mv}(h,T)\frac{\partial h}{\partial \hat{n}} + D_{tv}(h,T)\frac{\partial T}{\partial \hat{n}} = 0\\ L_0\rho_i q_v + c_v \rho_i q_v (T - T_0) = 0 \end{cases}$$
(4)

where  $\hat{n}$  is the unit outward normal vector along the boundary of a given soil profile. In the boundary conditions [Eq. (4)], the new vapor transfer model does not contribute to the water and heat fluxes between soil and ambient. That is because the water (both in liquid and vapor phases) and heat exchanges on the boundaries, such as evaporation, infiltration, or

solar radiation, have been fully expressed in  $M_{\rm prel}$  as "mass fluxes" and "energy fluxes", and solved before Eqs. (3) and (4). Therefore, the vapor transfer model can be considered as an "internal compensation" or "rebalance" of water and energy redistributions within the soil via vapor fluxes.

One benefit of using the boundary conditions [Eq. (4)] is that the boundary conditions originally employed in  $M_{\rm prel}$  do not need to be changed due to the inclusion of the vapor transfer model, which minimizes the potential changes of existing modules due to the implementation of the new vapor transfer module. However, the drawback is, if the boundary conditions [Eq. (4)] are assumed, the vapor transfer model must be executed after  $M_{\rm prel}$  and cannot work on itself, because no water and heat exchanges between soil and ambient are established in the new vapor transfer model via its own boundary conditions.

In the following sections, the combination of  $M_{\rm prel}$  and the new vapor transfer model [Eqs. (3) and (4)] is referred to as the "combined formulation ( $M_{\rm comb}$ )", where  $M_{\rm comb}$  is built on  $M_{\rm prel}$  and  $M_{\rm prel}$  becomes a sub-process of  $M_{\rm comb}$ .

By the end of this subsection, we summarize the positions of the four model formulations,  $M_{\text{prel}}$ ,  $M_{\text{comb}}$ ,  $M_{\text{simp}}$  and  $M_{\text{full}}$ .  $M_{\text{prel}}$  is an existing formulation with limited performance due to the lack of vapor transfer simulation. The new vapor transfer model is developed as a separate module and combined with  $M_{\mathrm{prel}}$  to obtain  $M_{\mathrm{comb}}$ .  $M_{\mathrm{comb}}$ , the new formulation proposed in this study, is a modularized soil water and heat simulator that includes vapor transfer. We expect  $M_{comb}$  can achieve similar performance as  $M_{\text{full}}$ .  $M_{\text{simp}}$  is an existing, simplified numerical formulation for the Philip and de Vries (1957) model. Since the main goal of this study is to combine  $M_{prel}$  with the new vapor transfer model to obtain  $M_{\rm comb}$  and evaluate the performance of  $M_{\rm comb}$  against  $M_{\rm full}$ ,  $M_{\text{simp}}$  does not belong to main target of this study. However, due to the wide adoption of  $M_{\text{simp}}$ , we included it for comparison. The four model formulations,  $M_{\text{prel}}$ ,  $M_{\text{comb}}$ ,  $M_{\text{simp}}$  and  $M_{\text{full}}$ , as well as the corresponding governing equations, are also summarized in Appendix B. In the next section, we will demonstrate the performance of  $M_{comb}$  by comparing  $M_{\rm comb}$  with  $M_{\rm prel},\,M_{\rm simp}$  and  $M_{\rm full}.$  With such comparisons, the efficacy of the new vapor transfer model, as a component in  $M_{\text{comb}}$ , can also be demonstrated.

### 2.3. Model demonstration for selected numerical examples

In this section, 1D illustrative examples implemented with Matlab (Mathwork, Inc.) are provided to demonstrate the efficacy of the new vapor transfer model, as well as the accuracy of  $M_{comb}$  in simulating soil water content and temperature. The accuracy of  $M_{\rm comb}$  can be evaluated by comparing the simulation results using  $M_{\rm comb}$  and the simulation results from  $M_{\text{prel}}$  and  $M_{\text{full}}$ . However, for the vapor transfer model, its performance is demonstrated through the performance of  $M_{\text{comb}}$ . That is, the accuracy of  $M_{comb}$  implies the effectiveness of the vapor transfer model, because the vapor transfer model is only one component (module) in  $M_{comb}$  rather than a completed water and heat simulator. Moreover, we note that the vapor transfer model is not designed to be executed on itself (In  $M_{comb}$ , the vapor transfer model must be executed after  $M_{\text{prel}}$ ), and pure vapor fluxes without any liquid water involved are rare in natural soil. Therefore, it will be challenging to provide error analyses for the new vapor transfer model on itself, with no liquid water flux included. Thus, we cannot use "accuracy" to quantify the performance of the vapor transfer model. In the following section, we will only use "efficacy" to represent the performance of the vapor transfer model, and we use "the vapor transfer model is effective" to indicate that  $M_{\rm comb}$ with the vapor transfer model can achieve errors smaller than  $M_{prel}$ , i.e.,  $M_{\rm comb}$  is more accurate than  $M_{\rm prel}$  with the new vapor transfer model

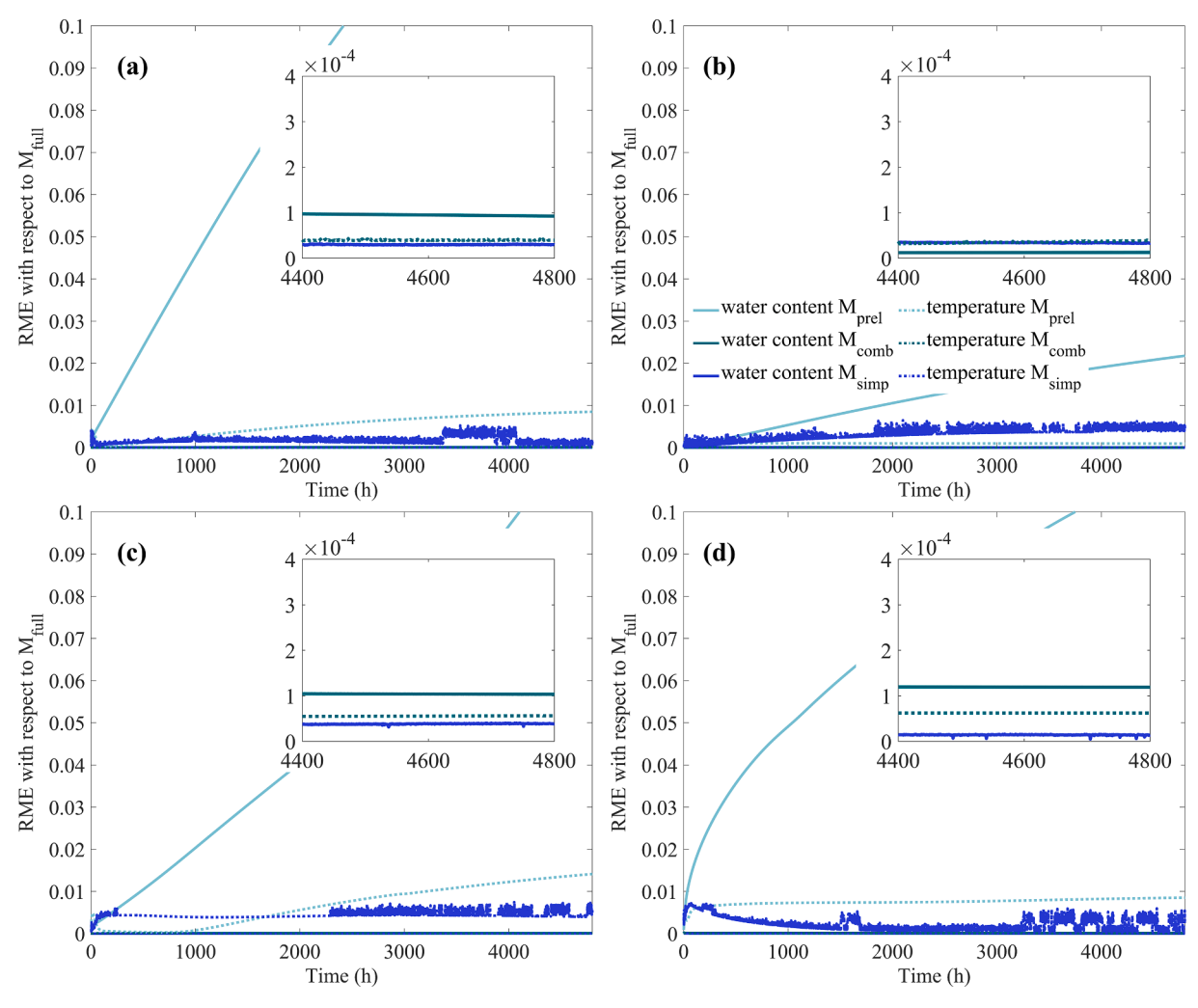


Fig. 1. The RME of simulated results using  $M_{prel}$ ,  $M_{comb}$  and  $M_{simp}$ , with respect to  $M_{full}$ , for four groups of stationary boundary conditions (a), (b), (c) and (d) in Table 2. The RME values are computed using Eq. (5). The large figures present the RME patterns for the whole simulations, while the associated small sub-figures emphasize the relatively small RME values of  $M_{comb}$  and  $M_{simp}$  as the simulations approach to the end (i.e., the time of 4800 h).

equipped.

A 50 cm horizontally placed soil column is used in the following numerical examples. The soil physical properties are isotropic and listed in Table 1. Such a setting (the selected soil type and the 1D simulation scenario) is used because the soil properties have been validated with both experimental and 1D numerical studies based on the Philip and de Vries (1997) model, and some existing applications also utilized the same soil type (e.g., Heitmann et al., 2008; Wang et al., 2017). Hence, the 1D simulation results via  $M_{\rm full}$  can be assumed as the "reference results".

The relative accuracy of  $M_{\rm prel}$ ,  $M_{\rm comb}$  and  $M_{\rm simp}$ , with  $M_{\rm full}$  as the reference, is presented based on the relative-mean-error (RME) of soil water content and temperature, i.e.,

$$RME = \frac{\sum_{k} |y_k - y_{k,full}|}{\sum_{k} |y_{k,full}|}, y = \theta \text{ or } T$$
(5)

In Eq. (5), y represents the simulated water content or temperature; the summation  $\Sigma_k$  is taken along the horizontal scale of the soil column, where k is the index of the node in a discretized computing grid. The subscript "full" indicates the results obtained using  $M_{\rm full}$ . The reason to use RME rather than the relative-root-mean-squared-error (RMSE) is to reduce the effects from large errors at single nodes. In this subsection, all

the model formulations, i.e.,  $M_{\text{prel}}$ ,  $M_{\text{comb}}$ ,  $M_{\text{simp}}$  and  $M_{\text{full}}$ , are solved on the same computing grid.

## Example 1. (Model comparisons with a series of steady boundary conditions)

In this example, we compared the simulated water content and temperature in the given 1D soil column for a series of steady boundary conditions, i.e., the boundary conditions do not change with respect to time. Four selected boundary conditions are shown in Table 2, including impermeable water boundaries [e.g., (a) and (b)], heat and water fluxes [e.g., (b) and (c)], and constant water content and temperature boundaries [e.g., (d)]. Those boundary conditions were selected to mimic a range of boundary conditions that may occur in agricultural fields or commonly used in numerical studies. Natural soils are seldomly adiabatic, so we do not include boundary conditions with zero heat fluxes, i.e.,  $q_h = 0$ . In this example, the boundary conditions are assumed to be steady; hence they can serve as constant external forces to drive the water and heat redistributions in soil. As  $t\to\infty$ , steady water content and temperature can be achieved within the soil column, which simplifies the error comparison. Therefore, the goal of this example is to show that  $M_{\rm prel}$ ,  $M_{\rm comb}$  and  $M_{\rm simp}$  can respond to the boundary conditions similarly to  $M_{\text{full}}$ .

The RME values of simulated results with respect to  $M_{\rm full}$  are pre-

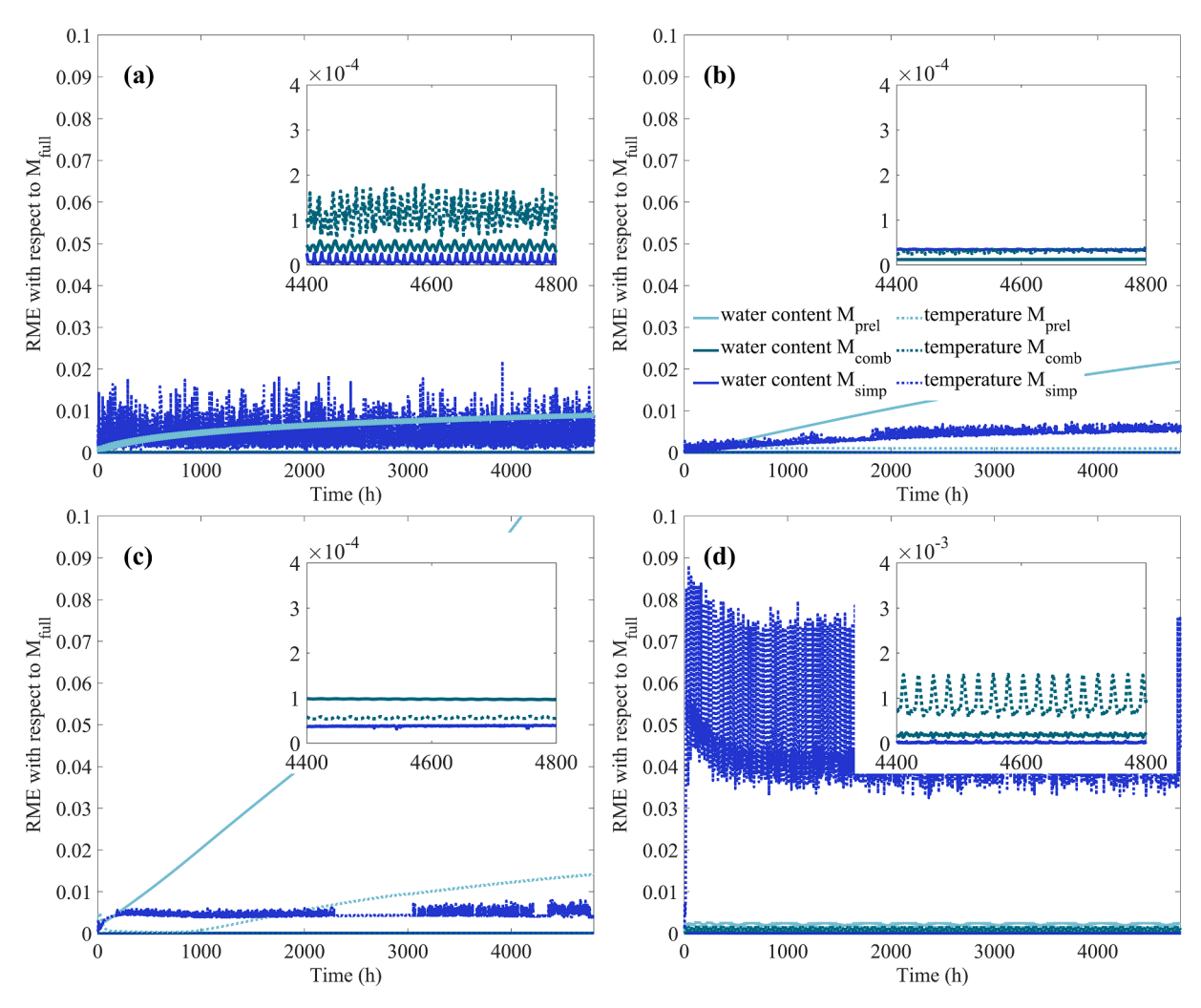


Fig. 2. The RME of simulated results using  $M_{prel}$ ,  $M_{comb}$  and  $M_{simp}$ , with respect to  $M_{full}$ , for four groups of time-dependent boundary conditions (a), (b), (c) and (d). The RME values are computed using Eq. (5). The large figures present the RME patterns for the whole simulations, while the associated small sub-figures emphasize the relatively small RME values of  $M_{comb}$  and  $M_{simp}$  as the simulations approach to the end (i.e., the time of 4800 h).

**Table 3**Initial and Boundary Conditions in Illustrative Example 2.

1111111111	tina Boundary G	JIIdition	o in mustrative Example 2.
(a)	Initial Condition		$ heta=0.15, T=25^{\circ} ext{C}$
	Boundary	Left	$q_l=0, q_ u=0, T=25^\circ ext{C}$
	Condition	Right	$q_l = 0, q_v = 0, T = 25 + 5\sin\left(\frac{2\pi t}{86400}\right)$ °C
(b)	Initial Condition		$\theta = 0.15, T = 25^{\circ}\text{C}$
	Boundary Condition	Left	$q_l = 0, q_{\nu} = 0, q_h = -0.0001 -$
			$0.00005 \sin\left(\frac{2\pi t}{86400}\right) \text{W cm}^{-2}$
		Right	$q_l=0, q_{\nu}=0, q_h=0.0001+$
			$0.00005\sin\left(\frac{2\pi t}{86400} + \pi\right) \text{W cm}^{-2}$
(c)	Initial Condition		$\theta = 0.20, T = 25^{\circ}\text{C}$
	Boundary	Left	$ heta=0.20, T=25^{\circ} ext{C}$
	Condition	Right	$q_l=0, q_{\nu}=-1\times 10^{-7}-2\times$
			$10^{-8} \sin\left(\frac{2\pi t}{86400}\right) \text{cm s}^{-1}, T = 30^{\circ} \text{C}$
(d)	Initial Condition		$\theta = 0.20, T = 25^{\circ}\text{C}$
	Boundary	Left	$ heta=0.20, T=25^{\circ} ext{C}$
	Condition	Right	$\theta = 0.20 + 0.10\sin\left(\frac{2\pi t}{86400} + \pi\right), T = 25 +$
			$5\sin\left(\frac{2\pi t}{86400}\right)$ °C

sented in Fig. 1. The relative error values with respect to  $M_{\rm full}$ , shown in the vertical axis, are calculated from Eq. (5). Although soil water content and temperature are not of the same dimension, the relative errors can be plotted together. The smaller the errors, the better the accuracy for the simulated results. The smoother the curves, the smaller the numerical oscillations.

In general, RME values of  $M_{\rm comb}$  and  $M_{\rm simp}$  are <0.005, indicating that both  $M_{\rm comb}$  and  $M_{\rm simp}$  can approximate  $M_{\rm full}$ . The small sub-figures show that when t is sufficiently large, the RME values of  $M_{\rm comb}$  and  $M_{\rm simp}$  do not approach 0. The reason is the governing equations corresponding to the two formulations,  $M_{\rm comb}$  and  $M_{\rm simp}$ , are not the same as the equations used in  $M_{\rm full}$  (see Appendix B for a summary). The RME values of  $M_{\rm comb}$  are small, indicating that ignoring the liquid water diffusion under temperature gradients is a reasonable assumption. In (a), (c) and (d), water content simulated with  $M_{\rm comb}$  has RME values of ~0.0001, which are greater than the RME values for  $M_{\rm simp}$ ; while in (b), the simulated water content with  $M_{\rm comb}$  achieves lower RME values than the simulated water content with  $M_{\rm simp}$ . Therefore,  $M_{\rm comb}$  and  $M_{\rm simp}$  can outperform each other under different simulation scenarios.

However, in all the four selected boundary conditions, the RME values of  $M_{\rm comb}$  simulated temperature are smaller than the RME values of the  $M_{\rm simp}$  results. One reason could be that the interaction between water and temperature transfer is simplified in  $M_{\rm simp}$ , where soil water content and temperature are updated by the two equations in Eq. (2')

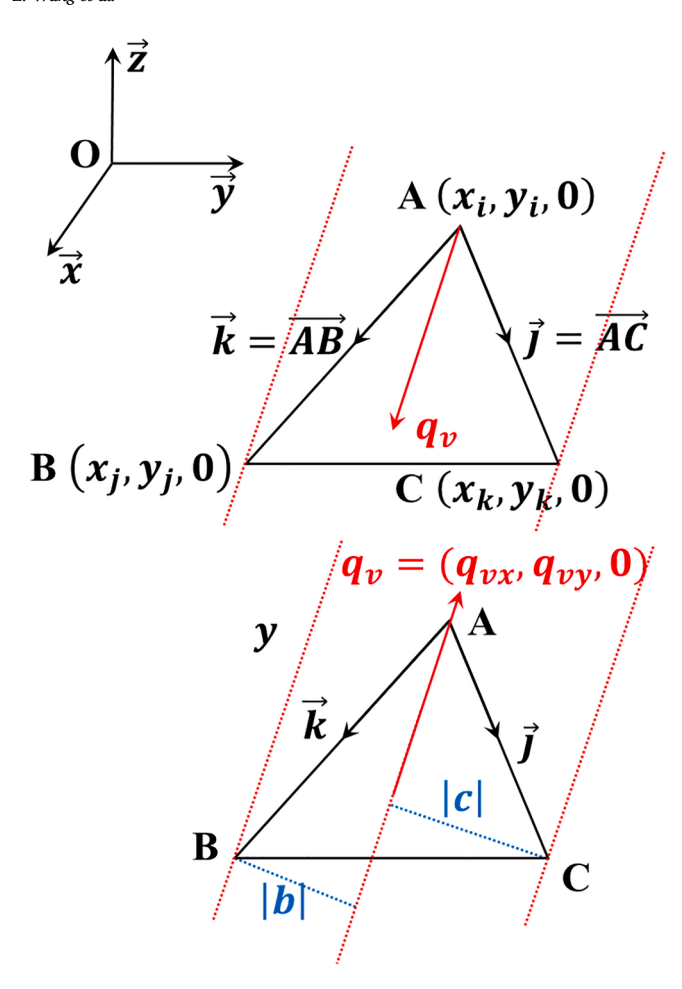


**Fig. 3.** Diagrams of the vapor fluxes within a given 2D triangular element in the x-y plane. Two examples of vapor flux directions based on node A are shown.

one-by-one. However, in  $M_{\rm comb}$ , although soil water content and temperature are first updated one-by-one in liquid water and heat transfer equations (i.e., the same as  $M_{\rm prel}$ ), soil water content and temperature are updated together in the vapor transfer model [Eq. (3)]. Therefore, some interactions between water and temperature are included.

Relatively large RME values can be observed in the  $M_{\rm prel}$  results for all four of the selected boundary conditions, except for the soil temperature in Fig. 2b. That is because, for all the simulation scenarios, temperature within the soil column is not uniformly distributed, and ignoring vapor transfer under temperature gradients, as well as the sensible and latent heat flux associated with vapor transfer can result in relatively large errors for both soil water and temperature. Soil temperature RME of the  $M_{\rm prel}$  results in Fig. 2b may be an isolated exception due to the certain type of boundary conditions; however, the corresponding soil water content RME values are still larger than other models. Therefore, we claim  $M_{\rm prel}$  still underperforms comparing with other formulations.

# Example 2. (Model comparisons for a series of time-dependent boundary conditions)

In this example, the boundary conditions vary with respect to time, with formulations shown in Table 3. The time-dependent boundary conditions are obtained by adding oscillation terms to the steady boundary conditions in Example 2 (some changes are made in the non-

oscillation parts to restrict soil water content between the residual and saturated water contents). As  $t\rightarrow\infty$ , soil water content and temperature, both within the soil profile and on the boundaries, are varied periodically following the oscillations in the time-dependent boundary conditions. Model evaluations with time-dependent boundary conditions are critical. The first reason is that physically, soil surface conditions in agricultural fields vary following the weather changes. The second reason is that numerically, interactions between water content and temperature can be presented in a single time step when solving  $M_{\text{full}}$ , because the two equations in Eq. (2) are fully coupled and the water content and temperature must be updated together. However, for  $M_{prel}$ ,  $M_{\text{comb}}$  and  $M_{\text{simp}}$ , water potential and temperature are solved one-by-one in a single time step, thus water and temperature interactions may need to be involved recursively with multiple time steps, which may induce "time-delays" and numerical oscillations. Therefore, the goal of this example is to determine whether  $M_{\text{prel}}$ ,  $M_{\text{comb}}$  and  $M_{\text{simp}}$  have a delayed response to the time-varying boundary conditions, compared to  $M_{\text{full}}$ , especially when the temperature and water content increase or decrease rapidly.

The RME values of simulated results with respect to  $M_{\rm full}$  are presented in Fig. 2. We observe relatively large fluctuations in RME values compared to those in Fig. 1, especially for  $M_{\rm simp}$  in (a) and (d) for the simulated soil temperature. Although  $M_{\rm simp}$  is able to reasonably reproduce the patterns of soil water and temperature, solving water content and temperature one-by-one leads to "time-delays" of minute-scale for the soil water and temperature, which induce periodic variations in the RME values with a relatively large magnitude under some boundary conditions (Fig. 2a and d).

We provide an intuitive interpretation for the "time-delays" and numerical oscillations in this example, due to the large magnitude of fluctuation in the RME values shown in Fig. 2a and d. Given a discrete time step  $\Delta t$ ,  $M_{\text{simp}}$  will first keep soil temperature constant and update soil water potential, where the soil water potential, as well as soil water content, can be solved using an iterative numerical method, such as Picard iteration. Second, soil water potential will be kept unchanged and soil temperature will be updated within  $\Delta t$ . The model formulation of  $M_{\text{simp}}$ , as well as the one-by-one updates of soil water potential and temperature are presented in Fig. 1 of Zheng et al. (2021). Within  $\Delta t$ , after the soil temperature is updated, the solution for the soil water potential and soil water content, obtained before the update of soil temperature, may not be optimal as it was, due to the change of soil temperature. However, in general,  $M_{\rm simp}$  will not allow solving the soil water potential again within  $\Delta t$ , but pushes the whole procedure to the next time step. Therefore, although the speed of convergence within  $\Delta t$ can be improved in  $M_{\text{simp}}$ , after completing the computation for  $\Delta t$ , there will be a slight error in the soil water potential due to such a "one-byone" approach. Similarity, because of the slight error in the soil water potential, soil temperature values solved in  $\Delta t$  may not be optimal either. Such errors will induce numerical oscillations in the RME values and can only be mitigated iteratively in the following time steps. In this study, such numerical oscillations are referred to as "time-delays". [We note that some realizations of Hydrus, e.g., Zheng et al. (2021), repeat the "one-by-one updates of soil water potential and temperature" for finitely many times (e.g., twice) within one time step. However, despite the increase in computing load, the convergence of soil water potential and temperature within each time step is still evaluated separately. The "time-delays" can be mitigated with such an improvement but may not be totally removed. In contrast, in  $M_{\text{full}}$ , the convergence of soil water potential and temperature must be evaluated as a whole within each discrete time step, see Appendix B for additional remarks].

Similar phenomena can also be observed in Fig. 1 for  $M_{\text{simp}}$ ; however,

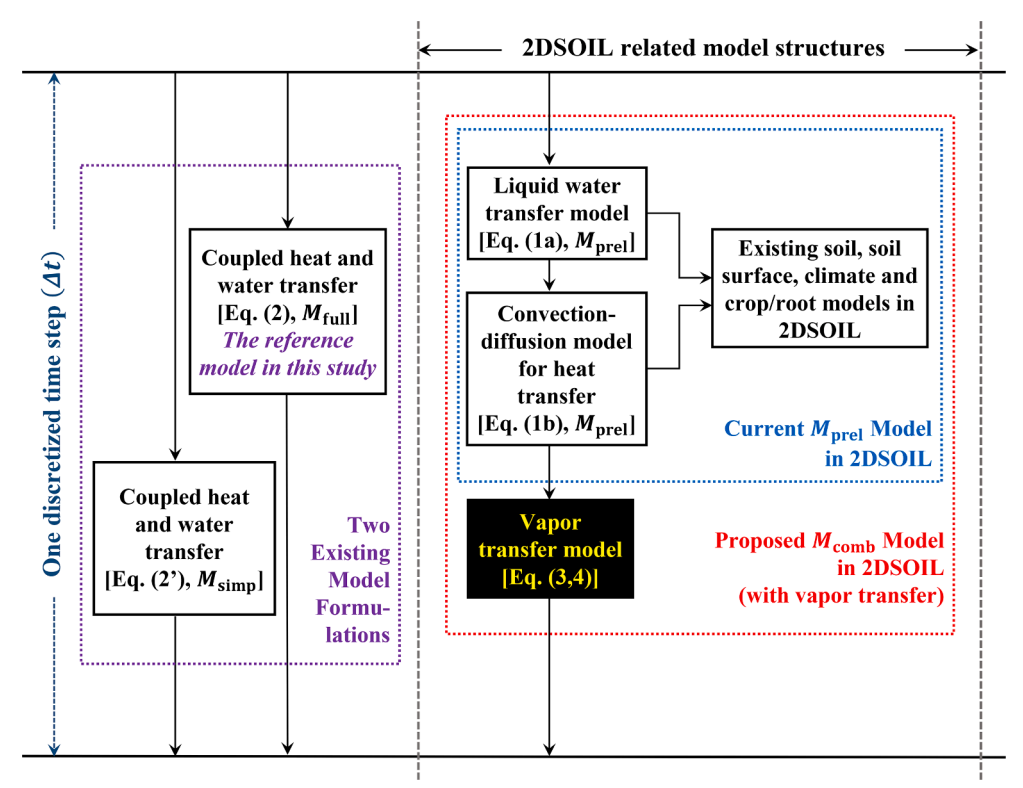


Fig. 4. The position of the new vapor transfer model (black box), as well as the layout of  $M_{\text{prel}}$  and  $M_{\text{comb}}$  in the 2DSOIL simulator, are shown. Each box presents modules. The new vapor transfer model is linked with M<sub>prel</sub> to include the water and heat redistributions induced by the vapor flux, and M<sub>comb</sub> is defined as the combination of M<sub>prel</sub> and the new vapor transfer model. The figure emphasizes the order of solving liquid water transfer, heat transfer and vapor transfer within a given time step  $\Delta t$  using  $M_{\text{comb}}.\ M_{\text{full}}$  and  $M_{\text{simp}}$  are also presented as two parallel model formulations.  $M_{\text{full}}$  and M<sub>simp</sub> has functions equivalent to M<sub>comb</sub>, while M<sub>full</sub> and M<sub>simp</sub> have additional functions (especially vapor transfer) compared to

**Table 4**Physical Properties of the Soil Used for the Simulations Described in Section 3.2.

J			
Alonzville (Fine-loamy, mixed, semiactive, mesic Typic Hapludults)			
Residual Water Content $(\theta_r, \text{cm}^3 \text{ cm}^{-3})$	0.052		
Saturated Water Content $(\theta_s, \text{cm}^3 \text{ cm}^{-3})$	0.376		
van Genuchten Parameter $(\alpha)$	0.028		
van Genuchten Parameter $(n)$	1.390		
Saturated Hydraulic Conductivity $(K_{sat}, \text{cm d}^{-1})$	23.541		
Soil Bulk Density $(\rho_b, \mathrm{g\ cm^{-3}})$	1.570		
Mass Fraction of Soil Organic Matter $(g g^{-1})$	0.006		
Mass Fraction of Sand (g g <sup>-1</sup> )	0.660		
Mass Fraction of Silt $(g g^{-1})$	0.180		

the magnitude of the RME fluctuations in Fig. 1 is much smaller than that in Fig. 2, because the boundary conditions in Example 1 are steady, so the numerical solution can recursively approach to the steady state of soil water and temperature. However, in Example 2, the boundary conditions are varying. Therefore, when  $M_{\rm simp}$  strives to reduce the "time-delays" produced in time step  $\Delta t$  using the following time steps, the boundary conditions are not the same as it was in  $\Delta t$ . Hence, the  $M_{\rm simp}$  may not be able to fully "catch up with" the changing boundary conditions.

In Fig. 2, the RME fluctuations for  $M_{\rm comb}$  are smaller than those for  $M_{\rm simp}$ . The reason is that in  $M_{\rm comb}$ , although the liquid water transfer and conduction–convection heat transfer are first solved one-by-one within  $\Delta t$  via  $M_{\rm prel}$  (recall  $M_{\rm prel}$  is the first step in  $M_{\rm comb}$ ), the vapor transfer model, as the next computing step in  $\Delta t$ , allows the soil water potential and temperature to be updated together one more time. Thus, the "time-delays" are partially avoided, and some interactions between soil water and temperature can be included via the vapor transfer model [refer to Eqs. (3) and (4)]. Hence the RME values for  $M_{\rm comb}$  are somewhat "smoothed".

For boundary conditions (a) and (d),  $M_{\text{prel}}$  seems to outperform  $M_{\text{simp}}$ ,

especially for the simulated soil temperature. That is because the periodic boundary conditions (a) and (d) only generate temperature variations within a relatively small slice of soil profile near the right boundary (where the boundary conditions vary), around the initial soil water content and temperature values. Therefore, in those cases,  $M_{\rm prel}$  becomes a rough approximation to  $M_{\rm full}$  from an average sense. Hence,  $M_{\rm prel}$  produces relatively small RME values.

In Examples 1 and 2, although  $M_{\rm comb}$  and  $M_{\rm simp}$  alternate on the best performance based on the RME values,  $M_{\rm comb}$  is more robust than  $M_{\rm simp}$  over all the scenarios. Because the accuracy of  $M_{\rm comb}$  implies the effectiveness of the new vapor transfer model, the good performance of the vapor transfer model is confirmed. Executing  $M_{\rm comb}$  requires solving two differential equation systems [Eq. (1) for  $M_{\rm prel}$  and Eq. (3) for vapor transfer]. Therefore, the computing load of  $M_{\rm comb}$  is larger than that for the other models in this study. However, such a drawback in computing load can be ameliorated by including parallel linear solvers, such as the oneAPI Math Kernel Library and the PARDISO solver (Intel Inc.) used in 2DSOIL.

#### 3. Implementation of the vapor transfer model in 2DSOIL

#### 3.1. Implementation of the vapor transfer model

Numerical implementation of the new vapor transfer model [Eqs. (3) and (4)] in 2DSOIL is presented in this section. The vapor transfer model is incorporated into the 2DSOIL and placed after the water and heat transfer modules to satisfy the  $M_{\rm comb}$  model formulation. 2DSOIL performs 2D numerical simulations based on a pre-generated triangular finite element grid. Soil water, heat and chemical transfer are programs with separate modules but solved on the same finite element grid. Therefore, following the existing water and heat transfer modules, numerical solutions of the vapor transfer model can be obtained on the same grid.

The performance of  $M_{\text{comb}}$ , as well as the vapor transfer model used in  $M_{\text{comb}}$ , have been validated in Section 2.3, so the main goal of Section 3 is to implement  $M_{\text{comb}}$  in 2DSOIL without strict comparisons with  $M_{\text{full}}$ .

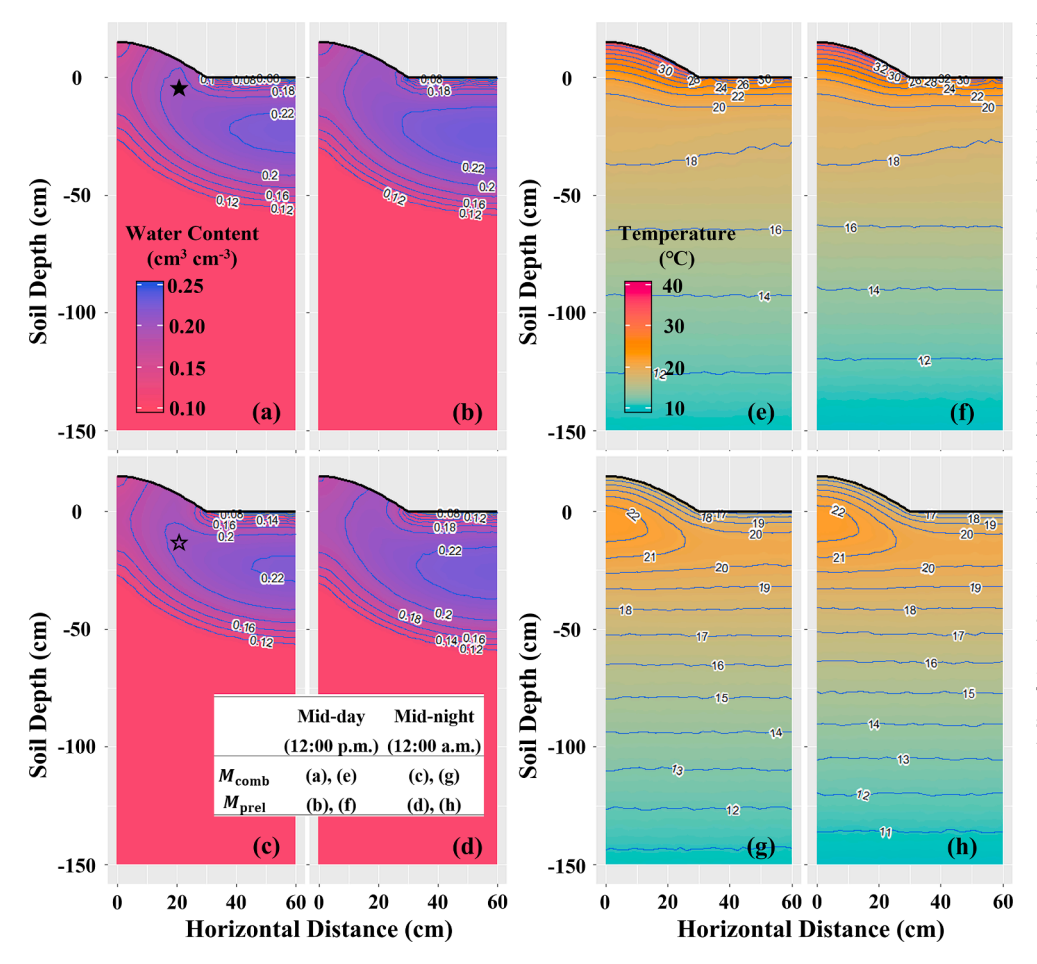


Fig. 5. The simulated soil water and temperature distributions using 2DSOIL with and without the new vapor transfer model. The soil includes a ridge surface covered by a plastic film and a bare flat surface, and the simulations are performed using observed weather data. Soil water and temperature distributions at mid-day and mid-night on a summer day (May 31, DOY = 140, 2017) are presented. The small table in the figure indicates the times (mid-day or mid-night) of the water and temperature results, and whether the vapor transfer model is ignored or invoked, i.e., M<sub>prel</sub> or M<sub>comb</sub>. (a) and (e) present the simulated soil water and temperature during the noon time using 2DSOIL with the vapor transfer module; (b) and (f) present the simulated soil water and temperature during the noon time using 2DSOIL without the vapor transfer module; (c) and (g) present the simulated soil water and temperature during the night time using 2DSOIL with the vapor transfer module; (d) and (h) present the simulated soil water and temperature during the night time using 2DSOIL without the vapor transfer module. Two labels "★" and "\parked the two small bends of the  $\theta=0.20~\text{cm}^3~\text{cm}^{-3}$  contours in (a) and (c).

Another reason for omitting the strict comparisons is that, were  $M_{\rm full}$  and  $M_{\rm simp}$  implemented in 2DSOIL, the modularized architecture in 2DSOIL will be lost and dataflow pathways will be substantially changed. Hence, the resulting simulator will operate much differently compared to the original 2DSOIL. Therefore, a directly comparison that including  $M_{\rm full}$  and  $M_{\rm simp}$ , under the 2DSOIL framework, cannot be applied.

For numerical schemes, the vapor transfer equation [Eq. (3a)] can be treated as a diffusive equation and solved by a standard finite element method. That is because the vapor advection, as well as the "liquid islands" effects that assist vapor transfer, can be included in the diffusive coefficient ( $D_{\rm IV}$ ) via a vapor enhancement factor (Cass et al., 1984). However, the heat transfer equation [Eq. (3b)] is a conduction-convective equation and should be solved with a conservative numerical scheme.

One simple way to establish a conservative scheme is to use the temperature from the upwind direction of the vapor flux on the righthand side of Eq. (3b). The upwind temperature  $(T_{up})$  can be determined for each triangular element in the 2DSOIL finite element grid. For example, consider an element that stays in the horizontal plane under the given coordinates in Fig. 3. First calculate the vapor flux,  $q_v = -D_{mv}(h,T)\nabla h - D_{tv}(h,T)\nabla T$ , where the water potential gradient  $(\nabla h)$  and temperature gradient  $(\nabla T)$  are obtained by linear interpolations, based on the water potential and temperature values at the grid nodes A, B, and C. Then, we analyze the vapor flux direction with respect to the three nodes.

For node A, if the triple products  $\overrightarrow{z} \cdot \left(\overrightarrow{k} \times q_{\nu}\right) > 0$  and

 $\overrightarrow{z} \cdot \left(q_v \times \overrightarrow{j}\right) > 0$ , i.e., the upper diagram in Fig. 3, a uniform vapor flux from node A to edge BC can be assumed to lie within the element and are demarcated by the two dotted red lines. Since A locates in the upstream direction of the vapor flux, the upwind temperature can be approximated by the temperature at A, i.e.,  $T_{up} = T_A$ . If the triple products  $\overrightarrow{z}$ .

 $\left(\overrightarrow{k} \times q_{\nu}\right) < 0$  and  $\overrightarrow{z} \cdot \left(q_{\nu} \times \overrightarrow{j}\right) < 0$ , i.e., the lower diagram in Fig. 3, a uniform vapor flux will occur from edge BC to node A, and the upwind temperature is a weighted average of the temperature at B and C, i.e.,  $T_{up} = (|b|T_c + |c|T_b)/(|b| + |c|)$ , where |b| and |c| are distances from B and C to  $q_{\nu}$ , respectively.

Similar procedures can be performed for nodes B and C to exhaust all the possible directions of the vapor fluxes. If the triple product is equal to 0, then the vapor flux is parallel to one of the edges, and the determination of the upwind temperature coincides with the method used in 1D upwind schemes. Substituting the temperature on the right-hand side of Eq. (3b) by the upwind temperature,  $T_{up}$ , Eq. (3b) can be discretized with the standard finite element method.

The diagram in Fig. 4 presents the position of the vapor transfer model in 2DSOIL and indicates how  $M_{\rm prel}$  and  $M_{\rm comb}$  are defined in 2DSOIL.  $M_{\rm full}$  and  $M_{\rm simp}$  are also presented. Fig. 4 indicates that the combination of the liquid water transfer model, the heat transfer model, and the new vapor transfer model in 2DSOIL, i.e.,  $M_{\rm comb}$ , performs a function equivalent to  $M_{\rm full}$  and  $M_{\rm simp}$ . Fig. 4 also emphasizes the order of solving liquid water transfer, heat transfer and vapor transfer within a given discretized time step  $\Delta t$  for  $M_{\rm comb}$  in 2DSOIL. The dataflow

pathways among the existing liquid water transfer module, heat transfer module, and other modules are maintained. No additional pathway is added after involving the vapor transfer model. Hence, the modularized architecture in 2DSOIL model is retained.

#### 3.2. An illustrative example of model applications

Because the effectiveness of the vapor transfer model and the accuracy of  $M_{\rm comb}$  have been demonstrated in Section 2.3, in this section, we provide an example to illustrate the simulation results of 2DSOIL with the new vapor transfer model, i.e.,  $M_{\rm comb}$ , and without the vapor transfer model, i.e.,  $M_{\rm prel}$ . Recall that  $M_{\rm full}$  and  $M_{\rm simp}$  cannot be easily supported based on the 2DSOIL framework. Thus, we only focus on  $M_{\rm prel}$  and  $M_{\rm comb}$ .

A 60 cm wide and 150 cm deep soil profile is considered, with the physical properties presented in Table 4. To provide spatial variations in soil water and temperature, a ridge is formed on the left 30 cm of the soil surface. The ridge has a 15 cm height, and the surface topography follows a cosine curve. Covered by a plastic film, the ridge surface becomes impermeable to water flux, but not to heat flux. The right 30 cm of the soil surface is flat and bare. During rainfall events, 94% of the precipitation received on the ridge becomes surface runoff, flows rightwards along the ridge surface, and infiltrates through the bare soil surface. This configuration is also referred to as the Ridge-Furrow Water Harvesting (RFWH), which is designed to conserve water in relatively deep soil layers (Wang et al., 2015; Zhao et al., 2018; Wang et al., 2020; Wang et al., 2021a).

Uniform initial water content (0.12 cm³ cm⁻³) and temperature (10 °C) are assumed in the soil profile, and the simulation is run for a 40-day period (DOY = 100–140 in 2017) to allow the soil profile to fully adapt to the ambient weather conditions. The water content and temperature distributions at 12:00p.m. (Mid-day) and 12:00 a.m. (Midnight) on the final simulation day (DOY = 140 in 2017) are recorded and presented in Fig. 5.

The differences in soil temperature between mid-day (Fig. 5e and f) and mid-night (Fig. 5g and h) can be observed. During the daytime (Fig. 5e and f), the soil surface receives radiation and achieves the highest temperature values. The temperature contours are nearly parallel to the soil surface, corresponding to an upwards temperature gradient. During the nighttime (Fig. 5g and h), the soil surface loses heat. Due to the plastic cover and the additional soil volume for the ridge, an area with relatively high temperature ( $T=22^{\circ}\text{C}$  contour) can be observed in the ridge. The benefit of including the vapor transfer model can be shown by comparing Fig. 5e and g, with Fig. 5f and h. The vapor flux carries sensible and latent heat flux from the soil surface to subsurface layers and increases the subsurface temperature. Therefore, the  $T = 12^{\circ}$ C contour in Fig. 5e (with vapor flux) is deeper than the T = $12^{\circ}$ C contour in Fig. 5f (no vapor flux), and the  $T = 12^{\circ}$ C and  $T = 13^{\circ}$ C contours in Fig. 5g (with vapor flux) are deeper than those in Fig. 5h (no vapor flux).

The effects of vapor transfer on soil water distribution can be observed by comparing Fig. 5a and c, and Fig. 5b and d. With the vapor transfer model invoked, during the daytime (Fig. 5a), the temperature gradient near the soil surface is relatively large, and the soil under the ridge has higher temperature than the soil under the flat surface. Therefore, temperature gradients drive vapor flux from the ridged portion to the flat portion, and lead to a small bend of the  $\theta =$  $0.20~\mbox{cm}^{3}~\mbox{cm}^{-3}$  contour in Fig. 5a near the ridge surface (marked with " $\star$ "), as well as a shrinkage of the  $\theta = 0.22 \text{ cm}^3 \text{ cm}^{-3}$  contour in Fig. 5a (with vapor flux) comparing to the  $\theta = 0.20 \text{ cm}^3 \text{ cm}^{-3}$  and  $\theta =$ 0.22 cm<sup>3</sup> cm<sup>-3</sup> contours in Fig. 5b (no vapor flux). In another words, the water vapor is "pushed" from the ridged portion to the flat portion of the soil profile due to the soil temperature gradient. During the nighttime, with the vapor transfer considered (Fig. 5c), the highest temperature occurs near the  $T=22^{\circ}$ C contour (see the position of  $T=22^{\circ}$ C contour in Fig. 5g), so the small bend of the  $\theta = 0.20 \text{ cm}^3 \text{ cm}^{-3}$  contour moves

from the soil surface in Fig. 5a to a location in Fig. 5c (marked as "\$\pi"), corresponding to the frontiers of the  $T=22^{\circ}\mathrm{C}$  and  $T=21^{\circ}\mathrm{C}$  contours in Fig. 5g (see the differences of  $\theta=0.20~\mathrm{cm^3}~\mathrm{cm^{-3}}$  contours in Fig. 5a and c for the changes of the contour shape and position). However, without considering vapor transfer (Fig. 5b and d), neither the small bends of the  $\theta=0.20~\mathrm{cm^3}~\mathrm{cm^{-3}}$  contour or its position changes, nor does the shrinkage (the decrease of internal area) of the  $\theta=0.22~\mathrm{cm^3}~\mathrm{cm^{-3}}$  contour occur (see the differences of the  $\theta=0.22~\mathrm{cm^3}~\mathrm{cm^{-3}}$  contours between "Fig. 5a and c" and "Fig. 5b and d" for the area enclosed within the contours). Without vapor transfer, the water transfer will only depend on the water potential distributions and have very limited response to the diurnal temperature changes. Hence, the water distributions in Fig. 5b and d are nearly identical. Therefore, the differences between  $M_{\mathrm{prel}}$  and  $M_{\mathrm{comb}}$  in simulating soil water distribution, as well as the effects of the new vapor transfer model, are illustrated.

#### 4. Summary

In this study, we design a numerical process to model the vapor flux and include vapor transfer effects on soil water and temperature simulations, when the liquid water transfer and heat transfer in soil are already considered. With the new vapor transfer model, simulations of liquid water, heat and vapor transfer in soil can be implemented as separate modules and solved one-by-one within a single discretized time step. The efficacy of the vapor transfer model, as well as the accuracy and stability of the coupled soil water and temperature simulations with the new vapor transfer model, are established via numerical experiments. The RME values of soil water content and temperature are < 0.005 relative to the standard Philip and de Vries (1957) model.

An advantage of using the new vapor transfer model is that for a modularized soil simulator where water and heat transfer modules exist but vapor transfer is not included, the vapor transfer can be easily added with minimal modifications to the existing modules or the dataflow pathways. The model formulation using the new vapor transfer model (i. e.,  $M_{\text{comb}}$ ) has a simple and flexible structure compared to the fully coupled formulation (i.e.,  $M_{\text{full}}$ ), and achieves stable simulation performance for most of the examples presented in this study. In this study, we implemented the vapor flow model in 2DSOIL, and a numerical example is presented to illustrate the effects of vapor transfer on 2D soil water and temperature regimes.

In conclusion, the vapor transfer model proposed in this study provides an effective and easy-to-use method to include vapor flux in soil water and heat transfer simulations. This study focuses on a new way to include vapor transfer into the soil water and heat simulations, and related applications, such as the vapor flux effects on chemical transfer and root growth, can be directions for future studies. Because adding the vapor transfer module leads to an increase in the computing load, the use of high-performance computing (e.g., parallel computing or GPU computing within personal computers) in soil water, heat and vapor transfer simulations is also encouraged and can be another possible direction for future research.

#### CRediT authorship contribution statement

Zhuangji Wang: Conceptualization, Formal analysis, Methodology, Software, Writing – original draft. Dennis Timlin: Conceptualization, Formal analysis, Methodology, Software, Writing – review & editing, Supervision. David Fleisher: Conceptualization, Supervision, Writing – review & editing. Wenguang Sun: Methodology, Software, Writing – review & editing. Sahila Beegum: Methodology, Software, Writing – review & editing. Sanai Li: Methodology, Software, Writing – review & editing. Yan Chen: Conceptualization, Supervision, Writing – review & editing. Vangimalla R. Reddy: Conceptualization, Supervision, Writing – review & editing. Katherine Tully: Conceptualization, Supervision, Writing – review & editing. Robert Horton: Conceptualization,

Supervision, Writing – review & editing.

#### **Declaration of Competing Interest**

The authors declare that they have no known competing financial interests or personal relationships that could have appeared to influence the work reported in this paper.

#### Acknowledgements

This material is based upon work supported by the Department of Agriculture, Agricultural Research Service under Agreement No. 58-8042-7-067, National Science Foundation under Grant 2037504, and USDA-NIFA Multi-State Project 4188. The authors also received support from the University of Maryland, College Park, University of Nebraska, Lincoln and Iowa State University.

#### Appendix A

The liquid water diffusion coefficient under temperature gradient  $[D_{tl}(h,T)]$  is used in model formulations  $M_{\text{full}}$  and  $M_{\text{simp}}$ . In this study, we ignored  $D_{tl}(h,T)$  in  $M_{\text{comb}}$  based on the assumption that  $D_{tl}(h,T) \ll D_{tv}(h,T)$ . Therefore, it is worth discussing that the formulation of  $D_{tl}(h,T)$  is namely treated as a diffusion coefficient based on the mathematical formulations of the partial differential equation models. However, physically, it should be considered as a "phenomenological coefficient" depending on the soil type (e Souza and Nogueira, 2020). Groenevelt and Kay (1974) and Milly (1982) proposed that liquid water transfer under temperature gradient was based on the variations of water-soil adhesion with respect to temperature and modeled it using "thermal-osmosis" and water surface tension, which was further simplified by Noborio et al. (1996). In this study, we apply additional simplifications to the model for coupled water and heat simulations.

Suppose the water surface tension ( $\sigma$ , N cm<sup>-1</sup>) is

$$\sigma = -7.275 \times 10^{-4} [1 - 0.002 \times (T - 291)] \tag{A1}$$

We artificially add a negative sign in front of the leading coefficient. That is because we assumed the soil is hydrophilic, so the negative sign indicates the suction from the soil capillary pores to liquid water, i.e., the strength of water tied to the capillary pores. Then, the temperature induced water potential change can be expressed as

$$\Delta h = \frac{\Delta \sigma(T) \times S_a \times S}{\rho_l \times g \times S} = \frac{\Delta \sigma(T) \times S_a}{\rho_l \times g} = \frac{S_a}{\rho_l g} \frac{\partial \sigma(T)}{\partial T} \Delta T \tag{A2}$$

In Eq. (A2),  $S_a(\text{cm}^2\text{ cm}^{-3})$  is the (volumetric) specific surface area of soil and  $S(\text{cm}^2)$  is the area of a given cross-sectional surface. Therefore,  $S_a \times S$  can be considered (approximately) as the perimeter of a liquid water film at the given cross-sectional surface, which is the simplification we proposed. Then, applying Eq. (A2) in Darcy's law, we have

$$q_{l} = -K(h, T)\nabla h = -\underbrace{\left[K(h, T)G_{a}\frac{S_{a}}{\rho_{l}g}\frac{\partial\sigma(T)}{\partial T}\right]}_{D(h, T)}\nabla T \tag{A3}$$

In Eq. (A3),  $G_a$  is an empirical gain factor with values ranging from 4 to 8, in general (Noborio et al., 1996). Because increasing the temperature can reduce the water-soil adhesion and increase the mobility of liquid water, the liquid water flux occurs from the regions with relatively high temperature to the regions with relatively low temperature. Following the expression of  $D_{tl}(h, T)$  in Eq. (A3),  $D_{tl}(h, T)/K(h, T)$  has an order of  $10^{-2}$ , which is of the same scale proposed by Prunty (2009). Lu et al. (2020) studied the transient soil water fluxes under a temperature gradient using a dual probe heat pulse method, with uniform initial soil water content and temperature. Lu et al. (2020) reported that under a range of initial soil water content and temperature, the liquid water transfer under temperature gradient is negligible, which provides additional evidence for the validity of our assumption that ignoring  $D_{tl}(h, T)$ .

In Appendix A, we presented a simplified approach to compute  $D_{tl}(h, T)$ . However, the model formulations in  $M_{\text{full}}$  and  $M_{\text{simp}}$ , as well as the general theory and numerical method proposed in this study are independent of the detailed empirical or physical expressions for  $D_{tl}(h, T)$ .

#### Appendix B

In this appendix, we provide a tabular summary for the governing equations corresponding to the model formulations, i.e.,  $M_{\text{prel}}$ ,  $M_{\text{comb}}$ ,  $M_{\text{simp}}$  and  $M_{\text{full}}$ , mentioned in this study. We note that the Philip and de Vries (1957) model serves as the foundation for all the formulations, expect for  $M_{\text{prel}}$ , which uses a simpler governing equation system. However, due to the designs of the model formulations, the governing equations that appear in  $M_{\text{comb}}$ ,  $M_{\text{simp}}$  and  $M_{\text{full}}$  may be different from the original, fully coupled version of Philip and de Vries (1957) model (Table B1).

#### Core Ideas.

- 1. A vapor transfer model is designed and applied for soil water and heat simulations.
- 2. Model performance is evaluated by its effects on coupled soil water and heat transfer.
- 3. The vapor transfer model is programed as a separate module in 2DSOIL.
- 4. 2DSOIL performs reasonable simulations with the vapor transfer model.

#### Declaration

- 1. The authors declare that they have no known competing financial interests or personal relationships that could have appeared to influence the work reported in this paper.
  - 2. This paper does not constitute a standard, specification, regulation, or recommendation for the numerical models and field management

 Table B1

 Summary of the Governing Models Mentioned in this Study (based on the order of first appearance in the paper).

Model	Equations for Each Formulation	Solving Procedures	Remarks
$M_{\mathrm{prel}}$	Water Equation: $\frac{\partial \theta}{\partial t} = \nabla \cdot [K(h, T) \nabla h]$ Heat Equation: $C_s \frac{\partial T}{\partial t} = \nabla \cdot [\lambda \nabla T] - \nabla \cdot [c_l \rho_l q_l (T - T_0)]$	<ul><li>(a) update soil water potential (or soil water content) using the "Water Equation".</li><li>(b) update soil temperature using the "Heat Equation".</li></ul>	$M_{\rm prel}$ is the starting point in this study, and $M_{\rm prel}$ does not include any form of vapor flux or vapor-induced heat flux.
$M_{ m full} \Biggl\{$	$\begin{aligned} &\textit{Water Equation}: C_{\theta\theta}\frac{\partial h}{\partial t} + C_{\theta T}\frac{\partial T}{\partial t} = \nabla \cdot \left[ \left[ D_{mv}(h,T) + K(h,T) \right] \nabla h + \left[ D_{tv}(h,T) + D_{d}(h,T) \right] \nabla T \right] \\ &\textit{Heat Equation}: C_{T\theta}\frac{\partial h}{\partial t} + C_{TT}\frac{\partial T}{\partial t} = -\nabla \cdot \left[ -\lambda \nabla T + c_{l}\rho_{l}q_{l}(T-T_{0}) + \left[ L_{0}\rho_{l}q_{v} + c_{v}\rho_{l}q_{v}(T-T_{0}) \right] \right] \end{aligned}$	Update both soil water potential (or soil water content) and soil temperature together within a given time step.	(a) $M_{\rm full}$ is the fully coupled formulation for soil water and heat transfer, with vapor transfer included. (b) Picard iteration is necessary during the updating of soil water potential and soil temperature. The convergence test used to exit the Picard iteration can be $\ h^b - h^a\ _{\infty} / \ h^a\ _{\infty} + \ T^b - T^a\ _{\infty} / \ T^a\ _{\infty} < \varepsilon$ where $a$ and $b$ indicate two consecutive iteration steps.
$M_{ m simp}$ $\langle$	$ \begin{cases} \textit{WaterEquation} : C_{\theta\theta} \frac{\partial h}{\partial t} = \nabla \cdot \left[ \left[ D_{mv}(h,T) + K(h,T) \right] \nabla h + \left[ D_{tv}(h,T) + D_{d}(h,T) \right] \nabla T \right] \\ \text{HeatEquation} : C_{TT} \frac{\partial T}{\partial t} = -\nabla \cdot \left[ -\lambda \nabla T + c_{l}\rho_{l}q_{l}(T-T_{0}) + \left[ L_{0}\rho_{l}q_{v} + c_{v}\rho_{l}q_{v}(T-T_{0}) \right] \right] \end{cases} $	<ul><li>(a) update soil water potential (or soil water content) using the "Water Equation".</li><li>(b) update soil temperature using the "Heat Equation".</li></ul>	$M_{ m simp}$ allows updating soil water potential and soil temperature in two steps.
$M_{ m comb}$	$\begin{cases} \text{Water Equation}: \frac{\partial \theta}{\partial t} = \nabla \cdot \left[ K(h, T) \nabla h \right] \\ \text{Heat Equation}: C_s \frac{\partial T}{\partial t} = \nabla \cdot \left[ \lambda \nabla T \right] - \nabla \cdot \left[ c_l \rho_l q_l (T - T_0) \right] \\ \\ \text{Vapor Equation}: \begin{cases} C_{\theta \theta} \frac{\partial h}{\partial t} + C_{\theta T} \frac{\partial T}{\partial t} = \nabla \cdot \left[ D_{mv}(h, T) \nabla h + D_{tv}(h, T) \nabla T \right] \\ \\ C_{T\theta} \frac{\partial h}{\partial t} + C_{TT} \frac{\partial T}{\partial t} = -\nabla \cdot \left[ L_0 \rho_l q_v + c_v \rho_l q_v (T - T_0) \right] \end{cases} \end{cases}$	<ul> <li>(a) update soil water potential (or soil water content) using the "Water Equation".</li> <li>(b) update soil temperature using the "Heat Equation".</li> <li>(c) update both soil water potential (or soil water content) and soil temperature together with the "Vapor Equation".</li> </ul>	(a) the first two steps in $M_{\rm comb}$ are exactly the same as they are in $M_{\rm prel}$ . (b) "Vapor Equation" corresponds to the vapor transfer model developed in this study. (c) $M_{\rm comb}$ is the only new model formulation established in this study, comparing to the existing model formulations, i.e., $M_{\rm prel}$ , $M_{\rm simp}$ and $M_{\rm full}$ .

#### techniques.

3. The computer code of the models included in this paper, as well as the input files of the illustrative examples, are released with the latest version of MAIZSIM at (https://github.com/ARS-CSGCL-DT, update recursively), a stationary executable version of the compute code is also available at (https://github.com/cauwzj).

#### References

- de Vries, D.A., 1958. Simultaneous transfer of heat and moisture in porous media. Trans. Am. Geophys. Union 39, 909–916. https://doi.org/10.1029/TR039i005p00909.
- Souza, K.B.e., Nogueira, C.d.L., 2020. Thermohydraulic flow problem in unsaturated porous media: FDM computational model. Int. J. Geomech. 20 (7), 04020101. https://doi.org/10.1061/(ASCE)GM.1943-5622.0001728.
- Cass, A., Campbell, G.S., Jones, T.L., 1984. Enhancement of thermal water vapor diffusion in soil. Soil Sci. Soc. Am. J. 48 (1), 25–32. https://doi.org/10.2136/ sssail984.03615995004800010005x.
- Groenevelt, P.H., Kay, B.D., 1974. On the interaction of water and heat transport in frozen and unfrozen soils: II. The liquid phase. Soil Sci. Soc. Am. J. 38 (3), 400–404. https://doi.org/10.2136/sssaj1974.03615995003800030012x.
- Heitman, J.L., Horton, R., Ren, T., Ochsner, T.E., 2007. An improved approach for measurement of coupled heat and water transfer in soil cells. Soil Sci. Soc. Am. J. 71 (3), 872–880. https://doi.org/10.2136/sssaj2006.0327.
- Heitman, J.L., Horton, R., Ren, T., Nassar, I.N., Davis, D.D., 2008. A test of coupled soil heat and water transfer prediction under transient boundary temperatures. Soil Sci. Soc. Am. J. 72 (5), 1197–1207. https://doi.org/10.2136/sssaj2007.0234.
- Kim, S.-H., Yang, Y., Timlin, D.J., Fleisher, D.H., Dathe, A., Reddy, V.R., Staver, K., 2012. Modeling temperature responses of leaf growth, development, and biomass in maize with MAIZSIM. Agron. J. 104 (6), 1523–1537. https://doi.org/10.2134/ agroni2011.0321.
- Lu, S., Ren, T., Horton, R., 2020. Estimating the components of apparent thermal conductivity of soils at various water contents and temperatures. Geoderma 376, 114530. https://doi.org/10.1016/j.geoderma.2020.114530.
- Lu, Y., Lu, S., Horton, R., Ren, T., 2014. An empirical model for estimating soil thermal conductivity from texture, water content, and bulk density. Soil Sci. Soc. Am. J. 78 (6), 1859–1868. https://doi.org/10.2136/sssaj2014.05.0218.
- Milly, P.C.D., 1982. Moisture and heat transport in hysteretic, inhomogeneous porous media: A matric head-based formulation and a numerical model, Water Resour. Res. 18 (3), 489–498. https://doi.org/10.1029/WR018i003p00489.
- Nassar, I.N., Horton, R., 1989. Water transport in unsaturated nonisothermal salty soil: II. Theoretical development. Soil Sci. Soc. Am. J. 53 (5), 1330–1337. https://doi.org/10.2136/sssai1989.03615995005300050005x.
- Nassar, I.N., Horton, R., 1997. Heat, water, and solution transfer in unsaturated porous media: I Theory development and transport coefficient evaluation. Transport Porous Med. 27, 17–38. https://doi.org/10.1023/A:1006583918576.
- Noborio, K., McInnes, K.J., Heilman, J.L., 1996. Two-dimensional model for water, heat, and solute transport in furrow-irrigated soil: II. Field evaluation. Soil Sci. Soc. Am. J. 60 (4), 1010–1021. https://doi.org/10.2136/sssaj1996.03615995006000040008x.
- Philip, R., de Vries, D.A., 1957. Moisture movement in porous materials under temperature gradients. Trans. Am. Geophys. Union 38, 222–232. https://doi.org/ 10.1029/TR038i002p00222.
- Prunty, L., 2009. Soil water thermal liquid diffusivity. Soil Sci. Soc. Am. J. 73 (3), 704–706. https://doi.org/10.2136/sssaj2008.0097.
- Richards, L.A., 1931. Capillary conduction of liquids through porous mediums. Physics 1 (5), 318–333.
- Saito, H., Šimůnek, J., Mohanty, B.P., 2006. Numerical analysis of coupled water, vapor, and heat transport in the vadose zone. Vadose Zone J. 5 (2), 784–800. https://doi.org/10.2136/vzj2006.0007.
- Scanlon, B.R., 1994. Water and heat fluxes in desert soils 1. Field study. Water Resour. Res. 30, 709–719. https://doi.org/10.1029/93WR03251.
- Scanlon, B.R., Milly, P.C.D., 1994. Water and heat fluxes in desert soils 2. numerical simulations. Water Resour. Res. 30 (3), 721–733. https://doi.org/10.1029/
- Simunek, J. and van Genuchten, M. T. 1994. The CHAIN\_2D code for simulating twodimensional movement of water flow, heat, and multiple solutes in variably

- saturated porous media. Version 1.1. Research Report No 136. Riverside, CA: USDA-ARS U.S. Salinity laboratory.
- Simunek, J., van Genuchten, M.T., Sejna, M., 2012. HYDRUS: Model use, calibration, and validation. Trans. ASABE 55, 1261–1274. https://doi.org/10.13031/2013.42239.
- Šimůnek, J., Genuchten, M.T., Šejna, M., 2016. Recent developments and applications of the hydrus computer software packages. Vadose Zone J. 15 (7), 1–25. https://doi. org/10.2136/vzi2016.04.0033.
- Sophocleous, M., 1979. Analysis of water and heat flow in unsaturated-saturated porous media. Water Resour. Res. 15 (5), 1195–1206. https://doi.org/10.1029/ WR015i005p01195
- Timlin, D., Pachepsky, Y.A., Acock, B., 1996. A design for a modular, generic soil simulator to interface with plant models. Agron. J. 88 (2), 162–169. https://doi.org/10.2134/agronj1996.00021962008800020008x.
- Vanderborght, J., Fetzer, T., Mosthaf, K., Smits, K.M., Helmig, R., 2017. Heat and water transport in soils and across the soil-atmosphere interface: 1. Theory and different model concepts. Water Resour. Res. 53 (2), 1057–1079. https://doi.org/10.1002/ wrcr.v53.210.1002/2016WR019982.
- Wang, Q., Ren, X., Song, X., Hu, G., Zhang, E., Wang, H., Vance, M.M., 2015. The optimum ridge–furrow ratio and suitable ridge-covering material in rainwater harvesting for oats production in semiarid regions of China. Field Crop. Res. 172, 106–118. https://doi.org/10.1016/j.fcr.2014.11.015.
- Wang, Z., Ankeny, M., Horton, R., 2017. The impact of water vapor diodes on soil water redistribution. J. Hydrol. 552, 600–608. https://doi.org/10.1016/j. ihydrol.2017.07.009.
- Wang, Z., Timlin, D., Kouznetsov, M., Fleisher, D., Li, S., Tully, K., Reddy, V., 2020. Coupled model of surface runoff and surface-subsurface water movement. Adv. Water Resour. 137, 103499. https://doi.org/10.1016/j.advwatres.2019.103499.
- Wang, Z., Timlin, D., Li, S., Fleisher, D., Dathe, A., Luo, C., Dong, L., Reddy, V.R., Tully, K., 2021a. Numerical simulations of maize root growth in MAIZSIM based on a diffusive model. Agri. Water Manag. 254, 106966 https://doi.org/10.1016/j. agwat 2021 106966
- Wang, Z., Thapa, R., Timlin, D., Li, S., Sun, W., Beegum, S., Fleisher, D., Mirsky, S., Cabrera, M., Sauer, T., Reddy, V.R., Horton, R., Tully, K., 2021b. Simulations of water and thermal dynamics for soil surfaces with residue mulch and surface runoff. Water Resour. Res. 57 (11) https://doi.org/10.1029/2021WR030431.
- Zhao, Y., Zhai, X., Wang, Z., Li, H., Jiang, R., Hill, R.L., Si, B., Hao, F., 2018. Simulation of soil water and heat flow in ridge cultivation with plastic film mulching system on the Chinese Loess Plateau. Agr. Water Manage. 202, 99–112. https://doi.org/10.1016/j.agwat.2018.02.017.
- Zheng, C.e., Šimůnek, J., Zhao, Y., Lu, Y., Liu, X., Shi, C., Li, H., Yu, L., Zeng, Y., Su, Z., 2021. Development of the Hydrus-1D freezing module and its application in simulating the coupled movement of water, vapor, and heat. J. Hydrol. 598, 126250. https://doi.org/10.1016/j.jhydrol.2021.126250.
- Zeng, Y., Su, Z., Wan, L., Yang, Z., Zhang, T., Tian, H., Shi, X., Wang, X., Cao, W., 2009a. Diurnal pattern of the drying front in desert and its application for determining the effective infiltration. Hydrol. Earth Syst. Sci (HESS) 13, 703–714. https://doi.org/ 10.5194/hess-13-703-2009.
- Zeng, Y., Wan, L.i., Su, Z., Saito, H., Huang, K., Wang, X., 2009b. Diurnal soil water dynamics in the shallow vadose zone (field site of China University of Geosciences, China). Environ. Geol. 58 (1), 11–23. https://doi.org/10.1007/s00254-008-1485-8.
- Zeng, Y., Su, Z., Wan, L.i., Wen, J., 2011a. A simulation analysis of the advective effect on evaporation using a two-phase heat and mass flow model. Water Resour. Res. 47 (10) https://doi.org/10.1029/2011WR010701.
- Zeng, Y., Su, Z., Wan, L., Wen, J., 2011b. Numerical analysis of air-water-heat flow in the unsaturated soil is it necessary to consider air flow in land surface models. J. Geophys. Res. – Atmosphere 116. https://doi.org/10.1029/2011JD015835.